Journal of Sound and Vibration (2002) **251**(5), 859–873
doi:10.1006/jsvi.2001.4017, available online at http://www.idealibrary.com on IDEAL®

A NEW METHOD FOR SIMULATING CONTACT FORCE BASED ON STATIC STRAIN EQUIVALENCE HYPOTHESIS

Y. ZHAO[†]

State Key Laboratory of Automotive Safety and Energy, Tainghua University, Beijing 100084, *People's Republic of China and*
CIMS Engineering Research Center, Tsinghua University, Beijing 100084, *People's Republic of China.*
E-mail; *yinyanz@263.net*

J. JIANG

Department of Engineering Mechanics, Northwestern Polytechnical University, Xi'an, Shaanxi 710072, *People's Republic of China*

AND

T. XIAO

CIMS Engineering Research Center, Tsinghua University, Beijing 100084, *People's Republic of China*

(*Received* 30 *November* 2000, *and in final form* 20 *August* 2001)

In this paper, a strain-based contact force simulation method (abbreviated as strain-based method or stain method) for low-velocity impact is proposed on the basis of static strain equivalence hypothesis, in which a strain ε at the contact point of a structure is selected as a quantity to evaluate the contact force. The procedure of this method is illustrated through a concrete example. The strain responses at different impact velocities calculated by the strain-based method are compared to the responses by the prediction method and by experiments, and the differences are analyzed. The results show that the responses from the former are much closer to the measured ones than those from the latter, especially when there exist some factors difficult to be considered in its theoretical model. So the proposed strain-based method is feasible and practical in research and engineering applications and the dynamic responses calculated by the method are of good stability and reliability. In addition, an existing prediction method is modified here based on the same hypothesis, and the modified results agreed well with the experimental results.

1. INTRODUCTION

In the field of dynamics, the contact force between an impactor and a target during impact often lasts only a few milliseconds and is very difficult to be traced. However, the correct description of the impact force history is all the time an important issue in related problems, for example, in the investigation for improving the resistance of composite materials to impact.

The correct description of impact force history is based on a clear understanding about second-split shock processes and can exert a large influence on the precision of the theoretical model of the system and the accuracy of its calculation results.

[†]Supported by Visiting Scholarship Foundation of Key Laboratory in Tsinghua University.

0022-460X/02/$35.00

Usually, the following two approaches are used to simulate contact force history. The first is Hertz's simulation method, and the second is the method of assuming the force history. Somehow, these two force history simulating approaches have their own advantages and limitations. They are introduced summarily here.

In the Hertz simulation method, the indentation α, defined as the local relative displacement between the impactor and the target, is separated from the displacements of other areas in the structure, and is regarded as a basic quantity used to evaluate the contact force F through a certain expression depending on α itself.

Originally, Hertz derived the classical contact law between an elastic sphere and an elastic half-plane. Ever since it was published it was used by many researchers in the impact problems of various isotropic materials. In the 1960s, Willis [1] obtained the exact expression of the contact force for a rigid sphere hitting a half-plane normally. The expression is

$$F = k\alpha^p, \tag{1}$$

where F is the contact force, α the indentation, and p and k are defined as indentation and contact indices respectively. These indices p and k can be obtained from experiments and are connected closely with the material properties of the sphere and the target and the radius of the sphere. In the 1980s, Tan and Sun [2] obtained a modified expression of the impact force suitable for laminated composite structures by modifying the above expression (1). The modified form is

$$F = k(\alpha - \alpha_0)^p, \tag{2}$$

where α_0 is the permanent indentation deformation. In this modification, the basic concept of Hertz's approximation law and the parameter α used to evaluate the contact force were not changed.

Being the basis of the Hertz indentation simulation method, the key point of the Hertz indentation approximation law is the assumption that the contact behavior between an impactor and a target under impact load is similar to that under static load. In other words, for the same specimen and under the same experimental conditions, the impact contact force corresponding to an indentation α is almost the same as the static contact force corresponding to the same indentation value.

From the explanations given above about the Hertz simulation method, it is clear that expressions (1) and (2) are in fact formulas validated by experimental data. On the one hand, this kind of expressions can include many experimental factors so that the force history can approximate the real one. On the other hand, the indentation between an impactor and its target is such an elusive value that the whole measuring device is complicate and the measuring task is heavy and therefore prone to errors. So the practical use of this method is strongly limited.

In the second, assuming contact force method, a known time function is adopted to describe the course of the contact force. Then the impact contact behavior becomes clear. For example, in reference [3], a simple prediction method for contact force history under low velocity impact (which will be introduced in detail in section 3 of this article, and will be simply called prediction method hereafter) was put forward. The advantage of this method is its easy implementation but it is obvious that the postulated function can be determined by pure theoretical computations after the system is given, and may simulate poorly the real conditions. So if the theoretical model of a system matches the real state very well, the dynamic responses calculated by this method will be acceptable, but conversely, if the model is not good in simulating the real states, the results will be affected by larger errors.

However, in engineering practice, the structural materials, shapes and constraints are often diverse and complex. This inevitably induces larger differences between the real contact forces and their assumed forms.

In view of these situations, researchers have been trying to find newer approaches for a better simulation of impact force.

2. STRAIN-BASED CONTACT FORCE SIMULATION METHOD AND ITS EXPERIMENTAL VALIDATION

2.1. STRAIN-BASED CONTACT FORCE SIMULATION METHOD AND ITS FOUNDATION

The strain-based contact force simulation method derived in this paper is very similar to the Hertz simulation method mentioned above. The key difference between them is that the former chose a strain ε at one point around the contact area of the structure rather than the indentation α, the relative deformation between impacting object and the target, as the basic quantity to evaluate the strength of the contact force.

The strain-based method is based on the static strain equivalence hypothesis, which was put forward in reference [4] and will be recalled here briefly. The static strain equivalence hypothesis consists in assuming that the relationships between an impact force F and a strain ε, at the center of the structure or around the force point, during impact and static processes are approximately identical. That is to say that the contact force F corresponding to a certain strain ε, at one point of the structure near the contact area, under low impact loading is approximately equal to the contact force corresponding to the same strain under static loading. This is very similar to the Hertz indentation approximate hypothesis.

In reference [4], the static strain equivalence hypothesis was verified through calculation and analysis in the range of low impact velocity. First, it was proved that a certain relationship existed between contact force and a strain, and the entire course of the relationship can be divided into three stages as shown in Figure 1. While loading, the strain varied almost linearly with the force (branch OA). When the force F reached its maximum value and began to decrease, the strain changed less than the force and showed a small

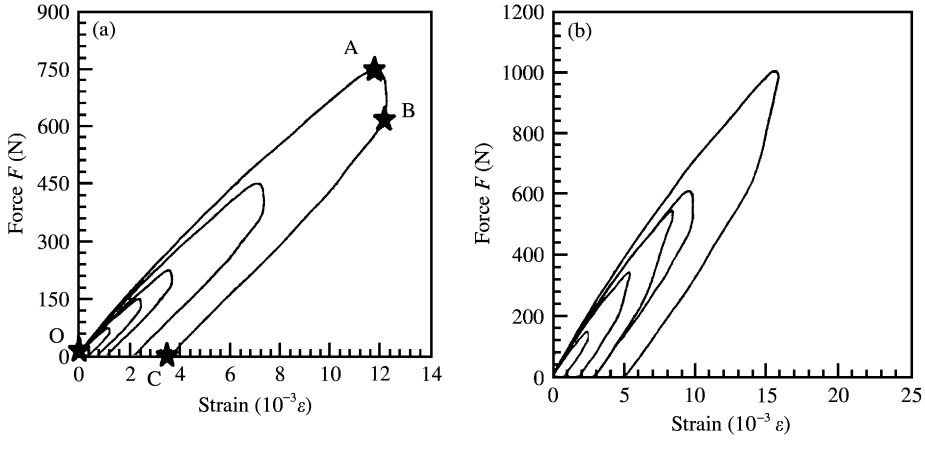

Figure 1. (a) Curves of F–ε_{0° at different impact velocities when mass ratio $\zeta = 0{\cdot}5$. $v_0 = 5{\cdot}0$, $3{\cdot}0$, $1{\cdot}5$, $1{\cdot}0$, $0{\cdot}5$, respectively from the outer to the inner; (b) Curves of F–ε_{0° at different mass ratios when $v_0 = 1{\cdot}0$ m/s. $\zeta = 2{\cdot}5$, $2{\cdot}0$, $1{\cdot}5$, $1{\cdot}0$, $0{\cdot}5$, respectively from the outer to the inner.

hysteresis at the beginning (branch AB). After the force F lowered 20–40% of its range, the strain again varied linearly until the force became zero (branch BC). Then, through calculation the proof was given that almost the same linear relations of F versus ε held during static and dynamic loading. The variation of their slopes is within 5%. Finally, a good stability of the above varying stages was obtained by inspecting the behavior of F–ε curves at different impact velocities and different mass ratios ζ (the impactor mass to the target mass), which can be observed in Figure 1(a) and 1(b).

Therefore, it was concluded that the static strain hypothesis was tenable in the range of lower velocities, and, on this basis, that the established strain-based simulation method is reliable and feasible. It is worth noting that in the entire impact history, if the small hysteresis is ignored, the F–ε curves during the loading and unloading courses show good symmetry.

2.2. PROCEDURE OF STRAIN-BASED CONTACT FORCE SIMULATION METHOD

To obtain the impact force history by using the strain-based method under low-velocity impact, the following three steps can be undertaken:

(1) *Static experimenting*. To draw the curve of contact force F versus a strain ε during static loading. The strain refers to a point at or near the force center of the target.

(2) *Dynamic experimenting*. To draw the response curve of the strain ε versus time t during impact loading.

(3) *Getting impact force history F–t from F–ε and ε–t curves*. Assuming that the relationship of static F–ε curve obtained in step 1 remains the same as dynamic F–ε curve while loading and combining it with the obtained dynamic response ε–t curve obtained in step 2, we can derive the first-half part of the force history, i.e., the F–t curve while the load is increasing. The whole force history will be completed by drawing the second-half part of the F–t curve according to the approximate symmetry of the impact history.

For a clearer explanation, an example is given here and the three steps mentioned above are applied to a concrete specimen to obtain its contact force history, which will be used in the later calculations and comparisons. The specimen is designed as follows.

Specimen A: Two-layered square plate with four clamped edges. Size: 200 mm × 200 mm. The upper and the lower layers are aluminum plates, the thickness of which is 0·5 and 2·0 mm respectively. The materials and their property parameters are listed in Table 1.

When utilizing the specimen in the experiments, in order to verify the comprehension of this force simulation method for the complex real situations, two rubber strips, 2 mm thick and 25 mm wide, were inserted between the clamp and the specimen on the border of its upper and lower surfaces. The rubber is regarded as the partial reflection to some complex real situations. A sketch is shown in Figure 2.

TABLE 1

Materials of the specimen A and their property parameters

Aluminum plates	Material model	Density ρ (kg/m^3)	Young's modulus E (GPa)	Shear modulus G (GPa)	The Poisson ratio v
Upper plate	LY12CZ	2800	68	26	0·33
Lower plate	LF21M	2730	70	27	0·296

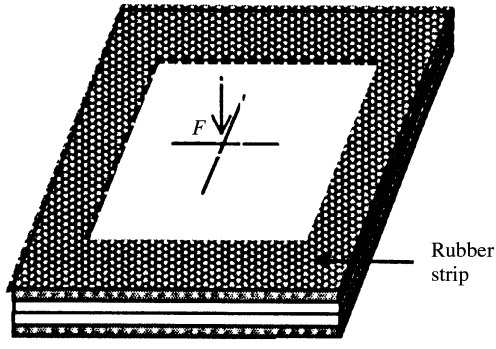

Figure 2. Sketch of the specimen used in the experiments.

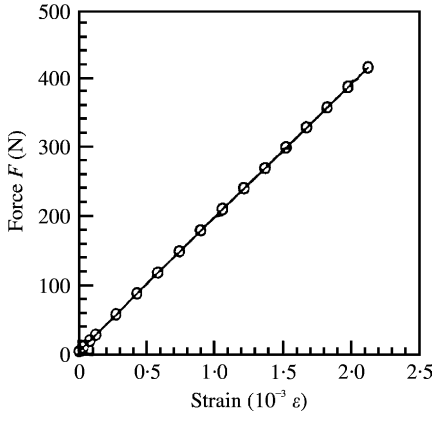

Figure 3. Experimental data and its fitted line of force F–ε_{0° in static loading.

In theoretical calculations, complex characteristics of real specimens, such as the rubber strips, are often discarded as their influences are not easily included into the calculation model.

We chose the center circular area of the square plate, with 6 mm diameter, which is also the diameter of the tip of the impactor, as our loading point, and chose the strain in 0°, or x direction at the center point of the lower surface of the plate, ε_{0°, as our object variable, setting one side of the plate parallel to 0° axis.

Step 1. Through static experimenting, the curve of contact force F versus the strain ε_{0°, F–ε_{0° curve, under static pressing can be drawn as shown in Figure 3. After curve fitting, a straight line with equation

$$\Delta F = 195{\cdot}5 \times 10^3 * \Delta\varepsilon \tag{3}$$

is obtained. In equation (3), the unit of F is Newton, while the strain ε_{0° is a dimensionless variable.

Step 2. Through dynamic experimenting, the real strain–time curve, ε_{0°–t curve, is drawn as shown in Figure 4 with dashed line. Its smoothed curve is plotted in Figure 4 with the solid line. The impact speed is $v_0 = 1{\cdot}50$ m/s.

Step 3. Taking the part of the ε_{0°–t curve obtained in step 2, from the starting-strain time to the maximum-strain time, and combining it with the F–ε_{0° curve obtained in step 1, we

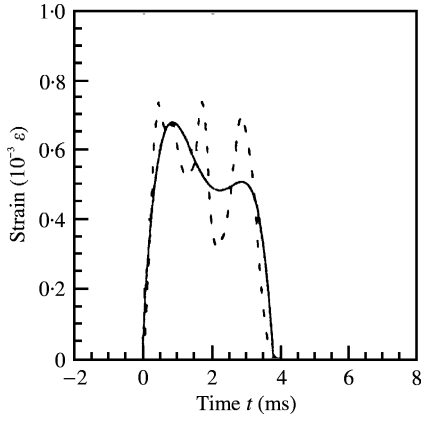

Figure 4. The solid line is the smoothed curve of measured ε_0–t curve at $v_0 = 1{\cdot}50$ m/s. The dashed line is the original curve.

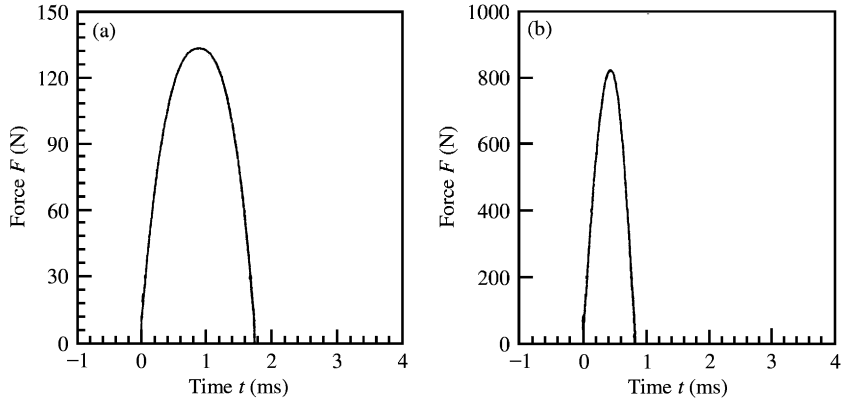

Figure 5. (a) Curve of contact force history by strain method at $v_0 = 1{\cdot}50$ m/s; (b) Curve of force history by prediction method at $v_0 = 1{\cdot}50$ m/s.

can obtain the first-half part of the force history. Extending this former part symmetrically we can derive the entire force history, F–t curve, which is drawn in Figure 5(a).

When calculating the dynamic responses of the system, the force at each time point then can be read out from the above F–t curve by interpolation.

2.3. COMPARISON OF STRAIN-BASED FORCE SIMULATION METHOD WITH THE PREDICTION METHOD

In order to examine the feasibility and precision of the new method for complex condition factors and experimental environments, the strain real-time responses of specimen A are calculated and measured experimentally. Calculations are made simulating the contact force by the proposed strain-based method and the prediction method, and their responses are compared with each other and with the experimental results. The specimen used in the work documented in this article is very similar to that discussed in reference [3], in which the prediction method was proposed, and both groups of constraints are the same.

In the following calculations, we adopted a model of the whole system, which consists of the layered plate and the impactor. For specimen A, we first consider the case when the impact velocity is $v_0 = 1{\cdot}50$ m/s. In Figure 5(a) and 5(b), two curves of force history for the same impact course are drawn, of which the former is obtained by the strain-based method and the latter by the prediction method. The maximum of the former curve is 135 N, while that of the latter is 810 N. The former plot has a lasting time of 1·7 ms, and the latter of 0·8 ms, that is to say that the force histories from the two different methods are rather different.

Now, let us turn to examine their dynamic responses. In Figure 6(a) and 6(b), all curves are the first periods of the first order harmonics of the strain real-time response ε_{0° under impact load. Plot No. 1 refers to the result calculated by the prediction method, plot No. 2 refers to the result calculated by the strain-based method and plot No. 3 refers to the smoothed measured strain response curve. For clear observation, curves No. 2 and No. 3 are illustrated at a larger scale in Figure 6(b), including the measured ε_{0°–t curve with dashed line, which is the original one and is not smoothed. As usual, we mainly care about the peak of the response curves. From Figure 6(a) and 6(b), the three peak values are read as 6·35, 0·82 and 0·74 ($10^{-3}\varepsilon$) corresponding to the results from the prediction method, the strain-based method and the measurements respectively. Obviously, the peak value obtained by the strain-based method is closer to the measured one, and that obtained by the prediction method is far larger than that by the other two.

The reason for the above large difference may be the insertion of rubber strips between the specimen and its clamp, which affect the dynamic responses by absorbing shock energy acting as a damper. However, the effect of these rubber strips is not considered in theoretical model of the system. Therefore, when the effect of the rubber strips is neglected, the computational dynamic responses will fit well the measured ones only when the contact force simulation closely models the experimental conditions. Otherwise, the computational responses will be far from the experimental ones.

The peak value of the response curve obtained by strain-based method matches well that of the smoothed measured curve mainly because in the strain-based method the force curve is derived from measured F–ε_{0° and ε_{0°–t plots and contains the comprehensive effect of all experimental factors such as the material properties of the system, the rigidity of the constraints and the characteristics of experimental devices. That is to say that some factors

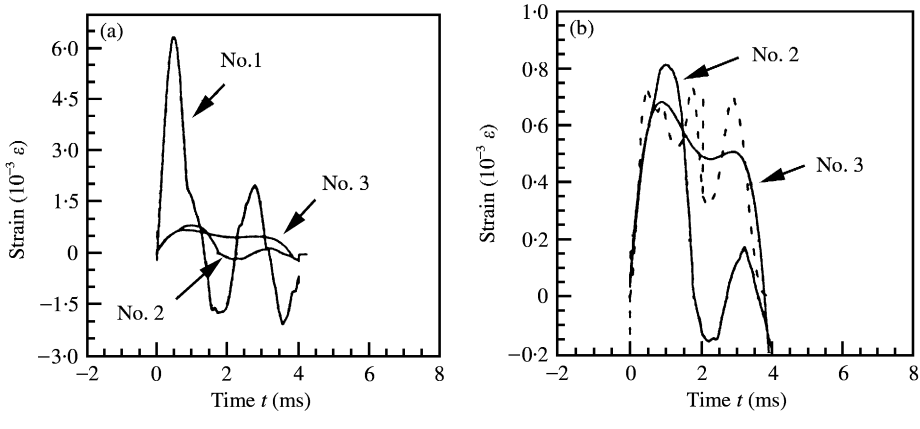

Figure 6. (a) Strain response curves ε_{0°–t at $v_0 = 1{\cdot}50$ m/s: (a) No. 1, computed by prediction method; No. 2, computed by strain method; No. 3, smoothed response curve; (b) No. 2, computed by strain method; No. 3, smoothed response curve; - - - the measured response.

that are difficult to be considered in a theoretical model can be accounted for in the final results through experiments and the force simulation approach. This explains the main advantages of this new strain-based method. Besides, the involved experiments are much simpler and easier than those involved in the Hertz method.

In addition, the three semi-period values of the first order harmonics are different, as it can be seen from Figure 6(a). The half-period obtained by the strain-based method becomes much longer than that derived from the prediction method due to the buffering effect of the rubber strips, even though it is still smaller than that obtained by experiments.

For the same specimen, the dynamic responses at another velocity, $v_0 = 2{\cdot}95$ m/s, are discussed and compared. The F–t curves obtained by the prediction method and by the strain-based method are given in Figure 7(a) and 7(b) respectively. The ε_{0°–t curves calculated by the two methods and the one smoothed from experimental data are drawn in Figure 8(a), marked as No. 1, No. 2 and No. 3 respectively. Curves No. 2 and No. 3 are illustrated at a larger scale in Figure 8(b), including the measured ε_{0°–t dashed curve.

By comparing the curves at $v_0 = 2{\cdot}95$ m/s in Figure 8 to the corresponding ones at $v_0 = 1{\cdot}50$ m/s in Figure 6, it follows that the pattern of each set of curves is identical, apart from the increase of their amplitudes with increasing impact velocity. So, compared to the experimental responses, the responses obtained by the strain-based method are still much

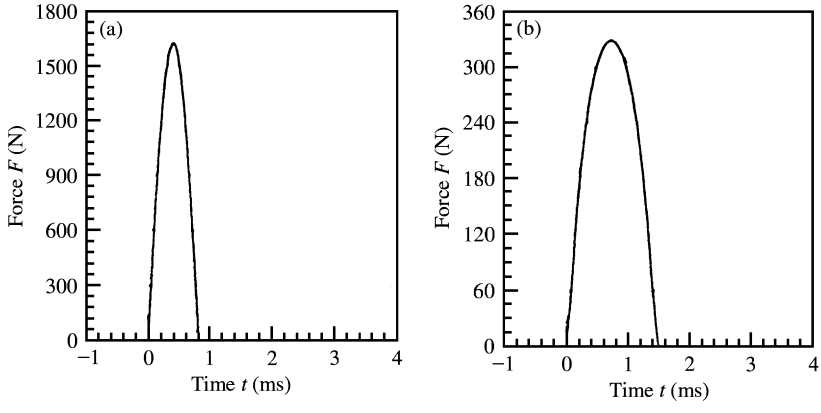

Figure 7. (a) Curve of force history F–t by (a) prediction method at $v_0 = 2{\cdot}95$ m/s; (b) strain method at $v_0 = 2{\cdot}95$ m/s.

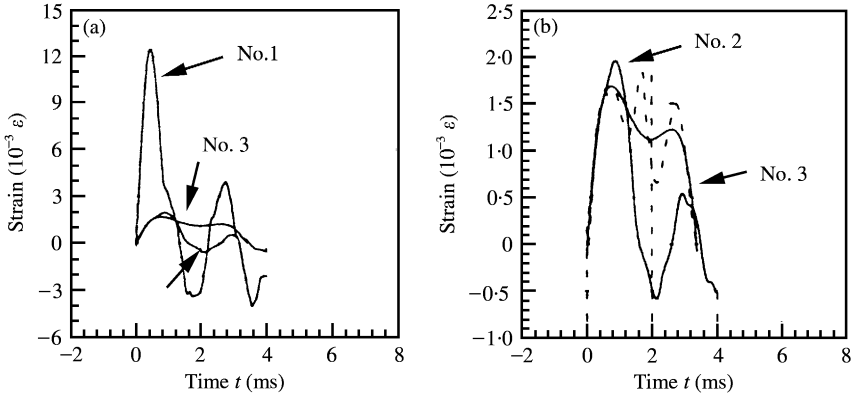

Figure 8. (a) Strain response curves ε_{0°–t at $v_0 = 2{\cdot}95$ m/s: (a) No. 1, computed by prediction method; No. 2, computed by strain method; (b) No. 2, computed by strain method; No. 3, the smoothed response curve.

TABLE 2

Force peak values, strain peak values and semi-periods of strain responses at different impact velocities

	Force peak values F_{max} (N)		Strain peak values $\varepsilon_{0^\circ max}$ ($10^3\mu\varepsilon$)			Half-periods of strain responses T_h (ms)		
Impact velocity (m/s)	Prediction method	Strain-based method	Prediction method	Strain-based method	Measured results	Prediction method	Strain-based method	Measured results
1.50	825·2	133·6	6·351	0·815	0·684	1·34	1·78	3·91
2·95	1626	329·3	12·52	1·936	1·685	1·34	1·60	3·38
97·1%	97·0%	195·7%	97·1%	140·8%	146·7%	0·0%	− 10·1%	− 13·5%

Note. Data in the last line are the percentage of the variation of the values from the first velocity to the second.

better than those obtained by the prediction method. The related data pairs obtained from the above figures are listed in Table 2. From this table, it may be seen that when the velocity changes from 1·50 to 2·95 m/s, the strain peaks increase by 140·8% as predicted by the new method, 97·1% by the prediction method, and 146·7% by the measured data. So, from the view of varied amount, the results from strain-based method are also better and their precision is satisfactory. The reduction of the semi-periods T_h of the responses (− 13·5%) obtained by the strain-based method is also closer to the reduction of the measured semi-periods.

So far, it is concluded firstly that the strain-based contact force simulation method is a practical and efficient method in low-velocity impact problems. It shows advantages especially when some factors are difficult to be considered in a theoretical model.

2.4. VERIFICATION UNDER DIFFERENT VELOCITIES AND AT DIFFERENT MEASURING POINTS

Observing the measured ε_{0°–t curves at several impact velocities plotted in Figures 9(a)–9(e), corresponding to $v_0 = 1{\cdot}50$, 2·10, 2·60, 2·95, and 3·60 m/s, respectively, we can see that the varying modes of measured strain responses are all the same within the range of low-velocity impact, although they show different peak values due to different impact energies. Combining these with all calculated responses at $v_0 = 1{\cdot}50$ and 2·95 m/s, we can further deduce that at any impact velocity, the response curve obtained by the new method and that obtained by the prediction method should be similar. Hence the curves referring to the strain-based method will be better, when compared to the experimental ones, than those obtained by the prediction method, in agreement with the conclusion drawn in the case of $v_0 = 1{\cdot}50$ and 2·95 m/s. That is to say the conclusion about the strain-based method drawn before is confirmed. So we can regard the calculation of the dynamic responses of the system by simulating the impact force with the strain-based method as feasible and reliable.

For global verification of the strain-based contact force simulation method, several other sample points, besides the central point, are positioned on the lower surface of the square plate. In consideration of the symmetry of the specimen, two groups of four strain flakes are stuck onto the plate along the 0° and 45° directions respectively. The distribution of the strain gauges is shown in Figure 10. From this figure, we can see that gauge 1 is located at

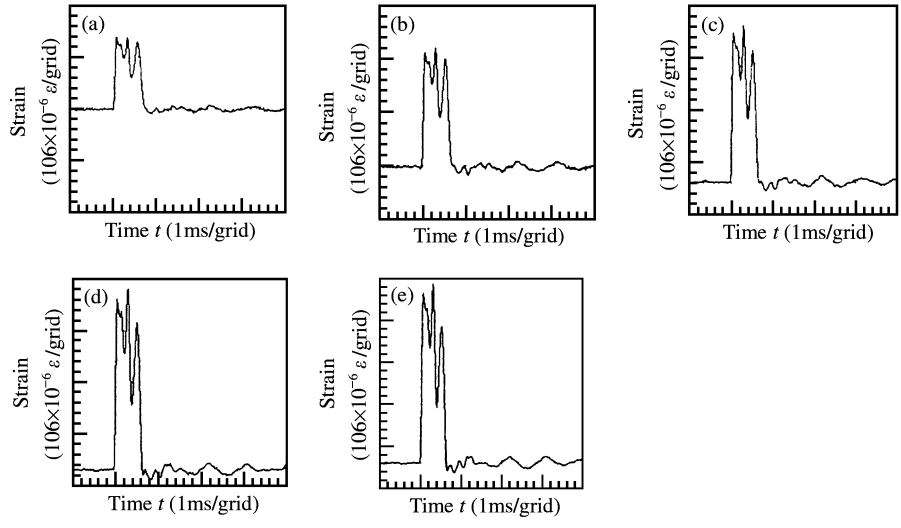

Figure 9. Measured ε_0–t curves at different velocities: (a) $v_0 = 1{\cdot}50$ m/s; (b) $v_0 = 2{\cdot}10$ m/s; (c) $v_0 = 2{\cdot}60$ m/s; (d) $v_0 = 2{\cdot}95$ m/s; (e) $v_0 = 3{\cdot}60$ m/s.

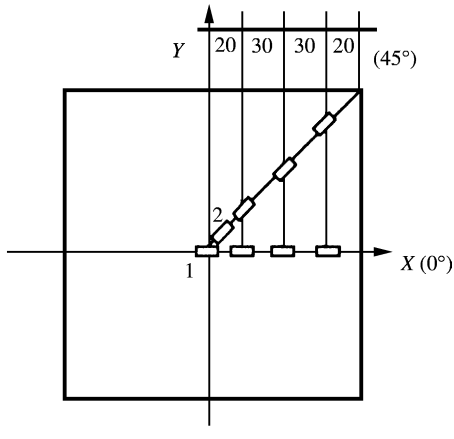

Figure 10. The distribution of the strain gauges on the lower surface of the specimen.

the center of the plate along the 0° line and gauge 2 is located about 5 mm from the center along the 45° line.

In Figure 11, which refers to the same speed values as those in Figure 9, are plotted the measured strain responses of gauge 2. By comparing the corresponding curves in Figure 11 for gauge 2 and Figure 9 for gauge 1, it becomes evident that apart from lower strain amplitudes for gauge 2 for a short distance from the center, a similar changing pattern is displayed for all couples of strain–time curves under each speed value. Moreover, a similar rising tendency is presented on the strain amplitudes of the two groups of curves with the speed rising. Then it is reasonable to infer that, just like with gauge 1, the dynamic strain response at the position of strain gauge 2 changes almost linearly with the contact force, as explained in section 2 of this article, but different slopes are displayed because of the different sample points. So the strain-based method can also be applied to this measurement.

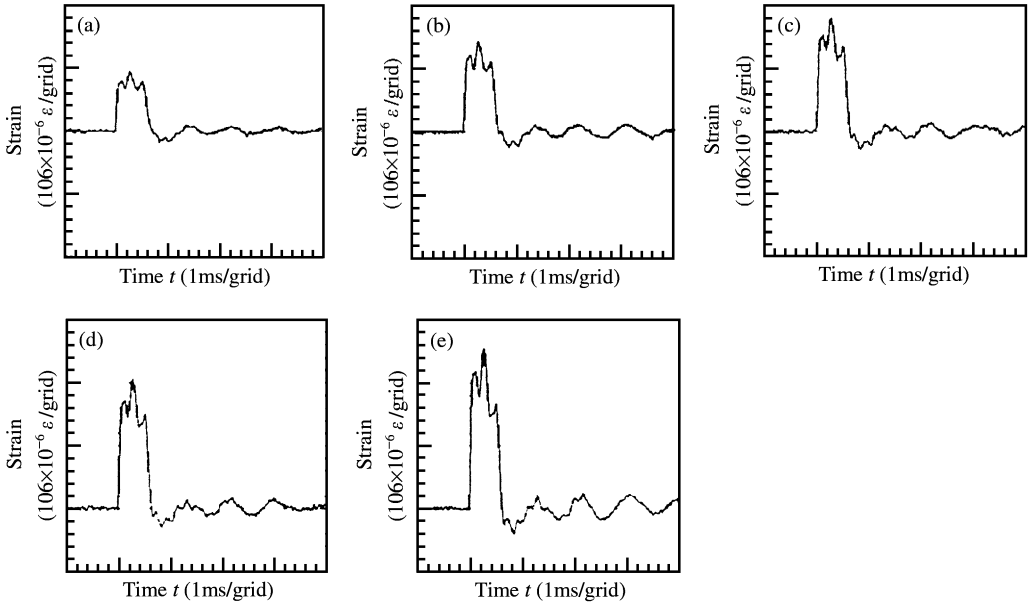

Figure 11. Measured ε_{45°–t curves at different velocities: (a) $v_0 = 1{\cdot}50$ m/s; (b) $v_0 = 2{\cdot}10$ m/s; (c) $v_0 = 2{\cdot}60$ m/s; (d) $v_0 = 2{\cdot}95$ m/s; (e) $v_0 = 3{\cdot}60$ m/s.

The results on other points around the center in any other directions can be deduced by analogy. However, measurement points at the center or near the center of the target are recommended strongly in the experiments for two reasons. One is that the amplitude of the strain in the center area is larger than that in points displaced from the center and then smaller relative errors are induced into the final results. The other is that the responses around the central area keep in phase with the main force pulse during contact, if a small hysteresis is ignored. However, in other points outside the center area the responses may be out of phase largely or even of opposite phase with respect to the main force pulse. In those cases, there may exist different relations between contact force and the strain response, a problem which is beyond the purpose of this article and therefore is not discussed here.

The above discussion confirms summarily that the strain-based method used to simulate the contact force history is feasible in research and engineering applications and that the dynamic responses of the structure under low impact velocities calculated by it are satisfactory and reliable.

In addition, if the desired precision for the simulation is not very high and when the strain-based method is adopted, the contact force histories under any other impact velocities can be derived from the experiments for only two velocities. This can be explained in the following by the typical instances in this article. For different impact velocities, it is obvious that an almost identical slope presents in the first stages of the F–ε curves in Figure 1(a), and it can be obtained from Figure 9 after a simple computation that a similar linear relation exists between the peak values of the first order strain responses and the impact velocities. Hence, a similar linear relation between the force peak value and the impact velocity can be derived. Then a similar force history pattern can be drawn for the specimen with different force peak values for different velocities. At least one F–ε curve and two ε–t curves are needed for getting the force pattern. This is in agreement with the basic theory of similar linear elasticity applicable to low-velocity impact. Otherwise, if the desired precision is very high, an experiment for each velocity is suggested. In related references

concerning the Hertz method, it is not seen whether experiments for more velocities can be omitted.

3. MODIFICATION OF THE PREDICTION METHOD

The prediction method mentioned before was put forward in reference [3]. The author gave a simple prediction for the impact force history when contact occurs only once. It is assumed that the deflection of the plate is small in comparison with its thickness and the system is similar to a spring–mass system. Therefore, the force history can be described as a sine function

$$F = \frac{2\pi m v_0}{T_1} \sin\left(\frac{2\pi t}{T_1}\right), \tag{4}$$

where T_1 is the first natural period of the system, t the contact time, m the mass of the impactor and v_0 the impact velocity. In the above expression, T_1 is fixed when the system is given, and the force amplitude is only dependent on v_0. So a change of the force range will influence the range of the corresponding deflection and strain responses, but will not influence the period of their first-class wave.

As was noted in the discussion in section 2, compared to experimental results, the errors of responses calculated by the prediction method are much larger than those obtained by the strain-based method. The main difference is found in their response peak values and it is caused directly by the large variation between the peak values of the force curves corresponding to the two methods. So, if the force peak obtained by the prediction method decreases, the strain peak will also decrease correspondingly. Therefore, the approach to reduce the response errors induced by the prediction method is to modify the amplitude of force expression in equation (4).

This modification is also on the basis of the static strain equivalence hypothesis and acts on the first part of the original sine function. Now, if we substitute the part before the sine function for F_{max}, then,

$$F = F_{max} \sin\left(\frac{2\pi t}{T_1}\right).$$

The steps necessary to derive F_{max} are almost the same as the three steps in the strain-based method explained in section 2. After getting F–ε and ε–T curves from experiments in step 1 and step 2, ε_{max} can be read out in an ε–T curve. Then F_{max}, which is defined as the force corresponding to ε_{max} in the F–ε curve obtained in step 3, can be read out. When the F–ε curve displays an approximate linear relation with slope $k_{F-\varepsilon}$, its exact form will be

$$F = \varepsilon_{max} k_{F-\varepsilon} \sin\left(\frac{2\pi t}{T_1}\right). \tag{5}$$

Now let us inspect the effect of this modification. Again for specimen A, and at $v_0 = 1{\cdot}50$, $2{\cdot}95$ m/s, its modified force histories are plotted in Figure 12(a) and 12(b), respectively, of which the corresponding originals are in Figures 5(b) and 7(b). Their strain response curves obtained through calculation and experiments are drawn in Figure 13(a) and 13(b), in which, plot No. 1 is the result obtained by the modified prediction method, plot No. 2 is the result obtained by the strain-based method and plot No. 3 is the smoothed measured response.

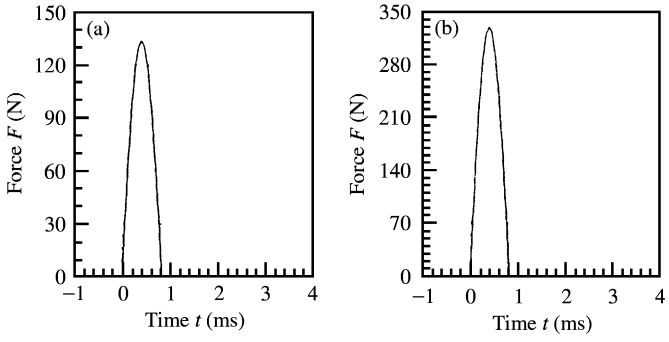

Figure 12. (a) Curve of force history F–t by modified prediction method at: $v_0 = 1{\cdot}50$ m/s; (b) $v_0 = 2{\cdot}95$ m/s.

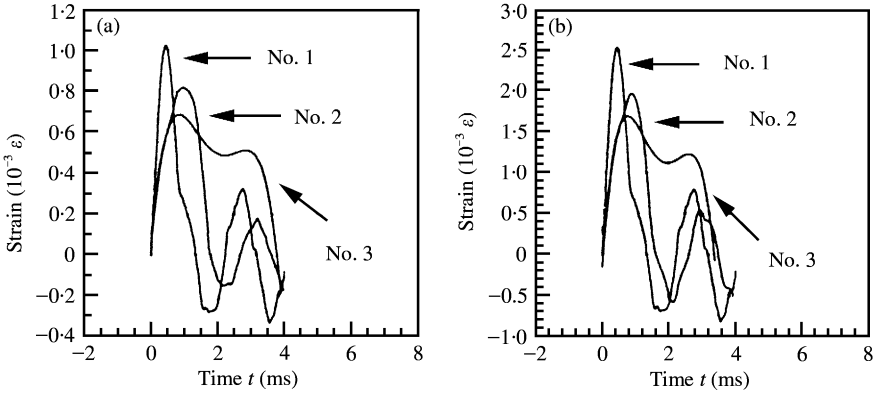

Figure 13. (a) Strain response curves ε_0–t at: (a) $v_0 = 1{\cdot}50$ m/s: No. 1, computed by modified prediction method; No. 2, computed by strain method; No. 3, smoothed response curve; (b) $v_0 = 2{\cdot}95$ m/s: No. 1, computed by modified prediction method; No. 2, computed by strain method; No. 3, smoothed response curve.

Some important data are listed in Table 3 for convenience. There is a marked drop of the force amplitude obtained by the prediction method after modification, 84% when $v_0 = 1{\cdot}5$ m/s, 80% when $v_0 = 2{\cdot}95$ m/s. The strain peak values obtained by the modified method drop by the same percentage and become 1·029 and 2·535 ($10^3\mu\varepsilon$) at the two velocities. These values are much closer than the originals, 6·35 and 12·52 ($10^3\mu\varepsilon$), to the experimental results, those are 0·6835 and 1·685 ($10^{-3}\varepsilon$), respectively. Also, these new results are very close to the results obtained by the strain-based method, 0·815 and 1·936 ($10^3\mu\varepsilon$) respectively. Therefore the modified prediction method can be considered as acceptable.

The force range obtained by the modified prediction method equals that predicted by the strain-based method because they are obtained in the same way. There is a small difference between the lasting time of the force histories in Figures 5(a) and 12(a) at $v_0 = 1{\cdot}50$ m/s, also in Figures 7(b) and 12(b) at $v_0 = 2{\cdot}95$ m/s, and this difference is the only dominant difference between the force histories obtained by the strain-based method and the modified prediction method, and therefore is the dominant error source of the dynamic responses derived by the two methods. Because this error is very small, we can say that the influence of the lasting time of the force on the responses is very limited.

Actually, that the results from modified method become closer to the measured results is also due to the fact that this method is closely related to experiments and practical

TABLE 3

Force amplitudes and strain amplitudes by different methods

Impact velocity (m/s)	F_{max} (N)			$(\varepsilon_{0^\circ max}$ $(10^{-3}\varepsilon)$			
	Unmodified method	Modified method	Strain-based method	Unmodified method	Modified method	Strain-based method	Measured result
1·50	825·2	133·6	133·6	6·351	1·029	0·815	0·6835
2·95	1626	329·3	329·3	12·52	2·535	1·936	1·685

experimental factors are implicitly accounted for in the calculation and eventually in the final dynamic responses.

4. SUMMARY

Both the strain-based contact force simulation method and the prediction method in the modified variant explained above are based on the static strain equivalence hypothesis. The steps taken in the strain-based method are not only strongly related to experiments, but also easy to accomplish through experimental measuring, so that the method is a practical one in research and engineering applications. The strain-based method is compared to the prediction method through experiments and calculations and the results show that this method is more reliable and of good precision. Therefore the strain-based contact force simulation method can be adopted and extended in future related engineering applications and research work. However, thus far, the strain-based contact force simulation method put forward in this paper and the static strain equivalence hypothesis advanced in reference [4] have been verified only in the range of low-velocity impacts, and only on typical specimens. It is necessary to promote further research on their theoretical basis, extend them to a larger scale and verify them in a wider range.

REFERENCES

1. J. R. WILLIS 1966 *Journal of the Mechanics and Physics of Solids* HERTZIAN contact of anisotropic bodies. **14**, 163–176.
2. T. M. TAN and C. T. SUN 1985 *Transactions of the American Society of Mechanical Engineers* **52**, 6–12. Use of statical indentation laws in the impact analysis of laminated composite plates.
3. I. H. CHOI and C. S. HONG 1994 *American Institute of Aeronautics and Astronautics* **32**, 2067–2075. New approach for simple prediction of impact force history on composite laminates.
4. Y. ZHAO, J. LIU and J. JIANG 2000 *Proceedings of the International Conference on Advanced Problems in Vibration Theory and Applications, June* 19, *Xi'an, People's Republic of China*. Static strain equivalence hypothesis for impact problem.
5. S. TIMOSHENKO and S. WOINOWSKY-KRIEGER 1959 *Theory of Plates and Shells*, 197–205. NewYork, Toronto, London: McGraw-Hill Book Company, Inc.
6. X. WANG and M. SHAO 1997 *Principle Theory and Numerical Method of Finite Element*, 395–420. Beijing: Tsinghua University Publishing Company.
7. H. AGGOUR and C. T. SUN 1988 *Computers and Structures* **28**, 729–736. Finite element analysis of laminated composite plate subjected to circularly distributed central impact loading.
8. K. J. BATHE and E. L. WILSIN 1976 *Numerical Methods in Finite Element Analysis*, 259–263. Englewood Cliffs, NJ: Prentice-Hall.

9. Z. ZHANG 1993 *Composite Structures Mechanics*, 15–119. Beijing Aerospace University Publishing Company.
10. L. B. GRESZCZUK 1982 *Impact Dynamics*. New York: John Wiley & Sons Inc.
11. R. CRAIG JR 1981 *Structural Dynamics*, New York: John Wiley & Sons Inc.
12. Y. QIAN and S. R. SWANSON 1990 *Composite Structures* **14**, 177–192. A comparison of solution techniques for impact response of composite plates.
13. H. V. LAKSHMINARAYANA, R. BOUKHILI and GAUVIN 1994 *Composite Structures* **28**, 47–59. Finite element simulation of impact tests of laminated composite plates.
14. A. B. CHAUDHARY and K. J. BATHE 1986 *Computers and Structures* **24**, 855–873. A solution method for static and dynamic analysis of three-dimensional contact problems with friction.